Polymer 125 (2017) 50–57

Contents lists available at ScienceDirect

Polymer

journal homepage: www.elsevier.com/locate/polymer

Flexible polydimethylsiloxane/multi-walled carbon nanotubes membranous metacomposites with negative permittivity

Kai Sun [a, b, c], Peitao Xie [b], Zhongyang Wang [b], Tongming Su [c], Qian Shao [d], JongEun Ryu [e], Xihua Zhang [b], Jiang Guo [c], Akash Shankar [e], Jianfeng Li [d], Runhua Fan [a, *], Dapeng Cao [f, **], Zhanhu Guo [c, ***]

[a] College of Ocean Science and Engineering, Shanghai Maritime University, Shanghai 201306, PR China
[b] School of Materials Science and Engineering, Shandong University, Jinan, 250061, PR China
[c] Integrated Composites Laboratory (ICL), Department of Chemical & Biomolecular Engineering, University of Tennessee, Knoxville, TN 37996, USA
[d] College of Chemical and Environmental Engineering, Shandong University of Science and Technology, Qingdao 266590, PR China
[e] Department of Mechanical Engineering, Indiana University-Purdue University Indianapolis, Indianapolis, IN 46202, USA
[f] State Key Laboratory of Organic–Inorganic Composites, Beijing University of Chemical Technology, Beijing 100029, China

ARTICLE INFO

Article history:
Received 2 July 2017
Received in revised form
27 July 2017
Accepted 30 July 2017
Available online 31 July 2017

Keywords:
Flexible metamaterials
Negative permittivity
Metacomposites

ABSTRACT

Metacomposites with negative electromagnetic parameters can be promising substitute for periodic metamaterials. In this paper, we devoted to fabricating flexible metacomposite films, which have great potential applications in the field of wearable cloaks, sensing, perfect absorption and stretchable electronic devices. The conductivity and the complex permittivity were investigated in flexible polydimethylsiloxane (PDMS)/multi-walled carbon nanotubes (MWCNTs) membranous nanocomposites, which were fabricated via in-situ polymerization process. With the increase of conductive one-dimension carbon nanotubes concentration, there was a percolation transition observed in conduction due to the formation of continuous networks. The dielectric dispersion behavior was also analyzed in the spectra of complex permittivity. It is indicated that the conduction and polarization make a combined effect on the dielectric loss in flexible PDMS/MWCNTs composites. The negative permittivity with a dielectric resonance was obtained, and was attributed to the induced electric dipoles.

1. Introduction

Metamaterials, termed as left-handed materials or double negative materials, are composed of artificially periodic unit cells and have drawn increasing attention owing to their exotic properties, such as negative refraction index [1], reversed Doppler effect [2] and reversed Vavilov-Cherenkov effect [3], which have promising applications in the field of invisible cloak [4], perfect lens [5], wireless power transfer [6] and magnetic resonance imaging [7], etc. Actually, due largely to the huge dissipation, complicated manufacture and narrow bandwidth [8], the development and applications of metamaterials with periodic building blocks were limited. Additionally, the negative electromagnetic parameters including permittivity and permeability are mainly controlled by their unit structures rather than their composition and microstructures of materials [9]. Therefore, as an alternative for periodic metamaterials, it is significant to construct random materials with negative electromagnetic parameters, which are called metacomposites [10] and have an isotropic electromagnetic response [11].

Compared with metamaterials, the tunable negative permittivity and/or negative permeability in metacomposites are dominated by tailoring their compositions and microstructures [12], which opens a novel approach to design metamaterials. It is demonstrated that negative permittivity behavior can be obtained resulting from the dielectric resonance of the polarization [13] or the plasma oscillation of the delocalized electrons in metallic clusters [11]. Nevertheless, the negative permittivity derived from metallic materials is usually enormous due to the ultrahigh electron concentration [14], which brings about impedance mismatch and

* Corresponding author.
** Corresponding author.
*** Corresponding author.
E-mail addresses: rhfan@shmtu.edu.cn (R. Fan), caodp@mail.buct.edu.cn (D. Cao), zguo10@utk.edu (Z. Guo).

http://dx.doi.org/10.1016/j.polymer.2017.07.083
0032-3861/

restricts their practical applications [15]. It is indicated that carbon materials can be a preferable substitute to achieve weak negative permittivity in bulk materials due to their moderate carrier concentration [16–19]. Furthermore, Shetty et al. [20] realized negative permittivity in bulk composites with carbon coated iron nanoparticle. Compared with bulk metacomposites, the membranous materials have greatly potential applications in the field of wearable cloaks [21], sensing [22], perfect absorption [23] and stretchable electronic devices [24], etc. In addition, there are few investigations with regards to flexible metacomposites with negative permittivity especially membranous materials. Therefore, in this paper, we devoted to fabricating flexible metacomposite films.

It is suggested that multi-walled carbon nanotubes (MWCNTs) have great potential applications in flexible electronics due to their high intrinsic carrier mobility, conductivity and mechanical flexibility [25,26]. Moreover, the commonly used substrates for flexible electronics are polydimethylsiloxane (PDMS) [27], polyimide (PI) [28] and polyethylene terephthalate (PET) [29] because of their suitable intrinsic properties such as lower permittivity and lower loss. However, PI has lower elastic regime due to its high Young's modulus, which reduces the tunability of metamaterials during mechanical deformations [30]. Meanwhile, a relatively high cross-link temperature (~400 °C) of PI may result in complications with functional fillers [31]. On the other hand, PET is susceptible to shear heat and has high cost, which is detrimental to its practical applications [30]. Compared with other materials [32–34], PDMS possesses outstanding elasticity, good mechanical property, excellent transparency and reliable nontoxicity [35,36], thereby it has become a promising candidate to make flexible, wearable and tunable devices [37].

In this paper, flexible and stretchable PDMS was used as matrix and multi-walled carbon nanotubes were selected as functional fillers to fabricate PDMS/MWCNTs nanocomposite films by in-situ polymerization method. The conductivity and the complex permittivity of the composites were investigated in the radio frequency region. With the increase of functional fillers, the electrical percolation phenomenon was observed in PDMS/MWCNTs membranous composites. The electrical conduction mechanism was further clarified. Moreover, the dielectric dispersion behavior of the complex permittivity was explored. Meanwhile, negative permittivity was achieved along with a dielectric resonance, where the permittivity switched from positive to negative. The mechanism to cause the negative permittivity was disclosed as well.

2. Experimental

2.1. Preparation process

The polydimethylsiloxane (PDMS)/multi-walled carbon nanotubes (MWCNTs) films were fabricated by in-situ polymerization process, the detailed schematic were shown in Fig. 1. The silicone elastomer base (Sylgard 184 A, Dow Corning Company) and curing agent (Sylgard 184B, Dow Corning Company) were mixed in the beaker with a 10:1 weight ratio, adding n-heptane (at the same weight of base) as the solvent. Subsequently, the mixture added with different mass fractions of MWCNTs without any treatment (0, 0.5, 2.5, 3.5, 5.0 wt%, which were denoted as samples PC-pure, PC-0.5, PC-2.5, PC-3.5 and PC-5.0). Furthermore, the MWCNTs were dispersed in the mixed solution by ultrasonic treatment at room temperature to reduce the agglomeration of MWCNTs; then the mixture was mechanically stirred at 600 rpm for 30 min.

After MWCNTs were uniformly dispersed into the matrix, the mixed slurry was coated on the smooth and clean glass substrate at a constant speed using the film applicator (Elcometer 3530); the thickness of the applicator was adjusted to 250 μm. Afterwards, the film with the glass substrate was put into the oven and dried at 353 K for 2 h. After polymerization process, the PDMS/MWCNTs film adhered to the glass substrate was took out from the oven. Subsequently, the coating and curing processes were repeated for additional five times with the film applicator. After totally cured, the film was peeled off from the substrate carefully. The PDMS film with uniformly dispersed MWCNTs was finally prepared by in situ polymerization.

2.2. Characterization and measurement

The phase composition of the film was analyzed by X-ray diffraction, a PANalytical X'Pert MPD PRO diffractometer equipped with a Si-based position-sensitive one-dimensional detector and Ni-filtered Cu Ka radiation source. The surface morphology and microstructure of the composite film were observed using SU-70 field emission scanning electron microscope (FESEM; Tokyo, Japan). The Fourier transform infrared (FT-IR) spectra of the pure PDMS and the composite film were obtained in the range of 500–4000 cm^{-1} at a resolution of 4 cm^{-1} using FT-IR spectroscopy (Bruker Inc. Vector 22, coupled with an attenuated total reflection (ATR) accessory).

The dc electrical conductivity for weakly conductive samples was tested by high resistance meter (Agilent 4339B, USA). For the samples with better conductive behavior, the dc electrical conductivity was measured by a four probe method. V-source testing mode (Keithley 2400 source meter, USA) was employed to make sure that a precise voltage was applied on the two inner probes. The measured voltage was adjusted in the range from −1 to 1 V, and the corresponding current was measured and recorded across the two outer probes [19].

The complex permittivity spectra were carried out at room temperature using an impedance analyzer equipped with 16453 A dielectric test fixture (Agilent E4991A, USA) in the frequency range from 10 MHz to 1 GHz. The films were tailored into wafers with a dimension of 25 mm in diameter for measurement. The silver paste was painted between samples and electrodes to eliminate the contact resistance. After calibration and compensation for the analyzer, the samples were placed between the two electrodes for measurement, at the action of a 100 mV ac voltage. The complex impedance ($Z = Z' + iZ''$) data were converted into capacitance C and resistance R for the complex permittivity ($\varepsilon = \varepsilon'_r + i\varepsilon''_r$) calculation, following equations (1) and (2),

$$\varepsilon'_r = \frac{Cd}{A\varepsilon_0} \tag{1}$$

$$\varepsilon''_r = \frac{d}{2\pi f A\varepsilon_0} \tag{2}$$

where Z' and Z'' are the real and imaginary impedance, ε'_r and ε''_r are the real and imaginary permittivity, C is capacitance, R is the resistance, d is the thickness of sample, f is the test frequency, A is the area of the electrode, and ε_0 is the permittivity of vacuum (8.85×10^{-12} F/m).

3. Results and discussion

Fig. 2 shows the FT-IR spectra of the pure PDMS and composite films with different MWCNTs loadings. For pure PDMS sample, the observed doublet peaks at 1100 cm^{-1} and 1020 cm^{-1} corresponded to the asymmetric and symmetric stretching vibration of two neighbor siloxane bonds [38]. Moreover, two obvious absorptions

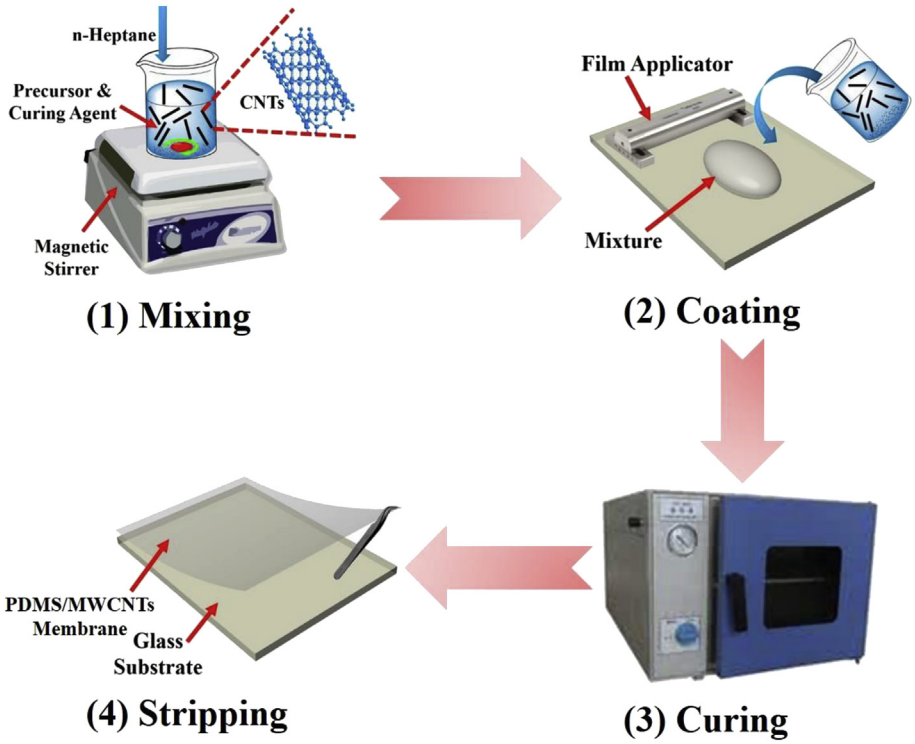

Fig. 1. The schematic of PDMS/MWCNTs membranous composites via in-situ polymerization process.

at 1259 and 800 cm^{-1} were related to the in-plane bending or scissoring and out-plane oscillations of the $Si-CH_3$ bonding, respectively [39]. Meanwhile, the methyl was observed at 2960 cm^{-1}, which means the asymmetric stretching vibration. After adding the MWCNTs fillers, the spectra of PDMS/MWCNTs films were in good accordance with that of pure film, indicating that there was no reaction between the two components. In addition, the molecular formula and 3D mode of PDMS molecule are shown in Fig. 2(b)-2(c), respectively.

The XRD patterns and SEM images of pure multi-walled carbon nanotubes and PDMS/MWCNTs composites are presented in Fig. 3. It was shown that there were two diffraction peaks observed at nearly 26° and 44° for pure MWCNTs(shown in Fig. 3(b)), which corresponded to (002) and (100) crystal faces, indicating the interlayer space in the radial direction and the in-plane graphitic structure of MWCNTs, respectively [40]. The XRD pattern of pure PDMS exhibited the amorphous structure with a distinct peak at around 12°, corresponding to the diffraction of the minicrystal of PDMS [41]. After adding the MWCNTs into the PDMS, the high intensity of PDMS masked the characteristic peaks of MWCNTs, which was hard to be recognized. With the increase of MWCNTs fraction, the diffraction peak of MWCNTs was gradually enhanced and the characteristic peaks did not shift (shown in Fig. 3(a)), also suggesting no chemical reaction during the curing process; that is to say, the PDMS/MWCNTs composites were successfully prepared by the in situ polymerization method. When the MWCNTs loading level was lower (shown in Fig. 3 (c)-3(d)), the fillers were randomly distributed in the matrix. Additionally, the MWCNTs were enclosed by the matrix, so carbon nanotubes were hard to be observed. With the increase of the MWCNTs content, the carbon nanotubes aggregated together and established a continuous network (in Fig. 3(e)-3(f)). The conduction behavior of a material is known to be very sensitive to its composition and microstructure [42]. Hence, the conduction behaviors of PDMS/MWCNTs composites are further investigated in the following section.

The dc conductivity of PDMS/MWCNTs films with the increase of filler fractions is shown in Fig. 4. For the pure PDMS film, the conductivity was as low as 5.19×10^{-15} Ω, presenting insulating property. After adding low content of MWCNTs fillers (0.5 wt%) into the matrix, the conductivity of the PDMS/MWCNTs film increased by less than one order of magnitude and it still possessed a weak conductivity. After the weight fraction of MWCNTs reached 2.5 wt%, the conductivity of the resultant film dramatically increased by almost eight orders of magnitude, indicating that there was an electrical percolation transition. Further increasing the conductive MWCNTs content, the conductivity got enhanced.

With the increase of conductive fillers content, the microstructure, distribution and topology of MWCNTs will generate obvious change [43]. As shown in the insets of Fig. 4, at low carbon nanotubes loading level, the one-dimensional fillers were randomly distributed in the matrix with a weak interconnection each other. When the concentration of functional fillers approached a threshold value f_c, the MWCNTs came into contact and formed a continuous percolating path throughout the insulating PDMS matrix [44]. Along with the change of microstructure, the conductivity of the composites also underwent an abrupt shift and the percolation behavior took place. The dependence of conductivity on filler content was corresponded to power law, which is described as equation (3) [45],

$$\sigma \propto |f - f_c|^{\pm e} \tag{3}$$

where σ is the conductivity of composites, f_c is the percolation threshold, f is the volume content of conductive fillers and e is a critical exponential parameter.

Generally, the distribution of fillers in a matrix plays an important role in determining the percolation threshold, which is attributed to the geometric parameters, such as particle size, shape, and orientation [43,45]. For the one-dimensional fillers with large

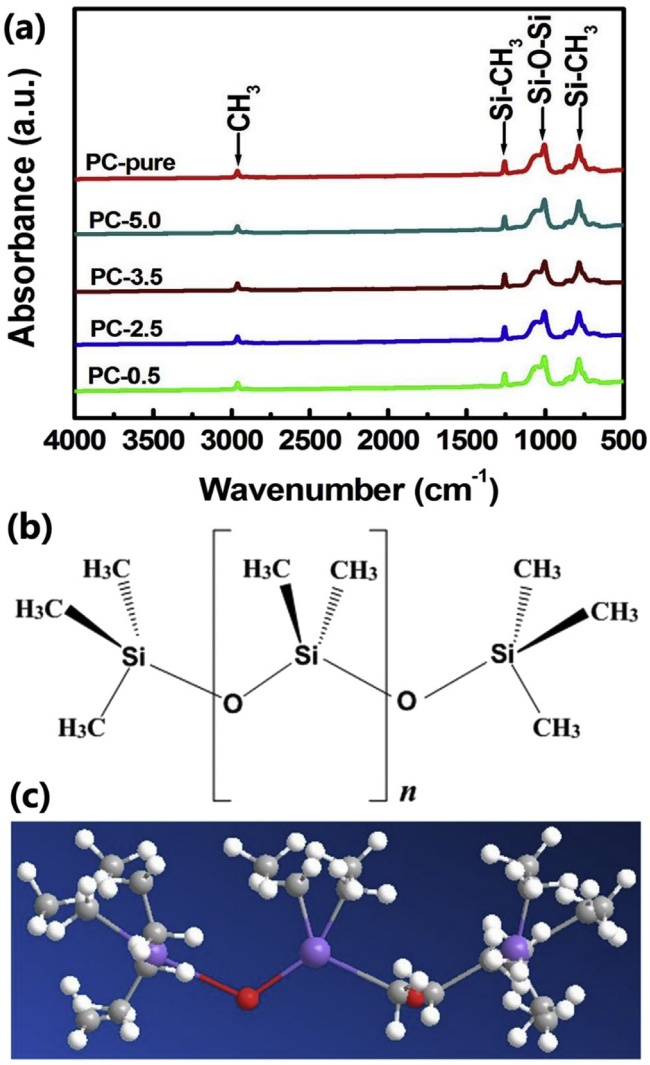

Fig. 2. The FT-IR spectra (a) of the pure PDMS and PDMS/MWCNTs film. (b) and (c) are the molecular formula and 3D mode of PDMS molecule, respectively.

aspect ratio, such as rods [46], tubes [47] or fibers [48], the percolation threshold was reduced significantly owing to the easier formation of conductive networks. Actually, the percolation threshold of PDMS/CNTs film was not located at a very low level due largely to the high polarity, high surface tension and a lower degree of crystallization of polymer matrix [49,50], which inhibited the uniform distribution of MWCNTs fillers in the matrix and resulted in a relatively high percolation threshold.

When the MWCNTs content was below the percolation threshold, the isolated fillers were randomly distributed in the PDMS matrix without forming percolation networks. Hence, the electrons just moved by discontinuous hopping along adjacent MWCNTs, following a hopping conduction mechanism [51]. After the concentration of MWCNTs fillers approaches a percolated state, the percolation network was established throughout the system and the electrons can move along the conductive networks, following a metal-like conduction behavior in the percolative composites [52,53].

The frequency dispersions of the complex permittivity and the dielectric loss for PDMS/MWCNTs composite are shown in Fig. 5. For the pristine PDMS, the dielectric constant was very low and the permittivity spectrum was nearly independent of frequency. When a low MWCNTs fillers loading (for example 0.5 wt%) was added, the real permittivity of the composite film got slightly enhanced. Further increasing the functional filler content, the dielectric constant of resultant film was markedly improved (shown in Fig. 5(a)), which was attributed to the Maxwell-Wagner-Sillars effect [44]. As is well known, when the conductive fillers were distributed in the matrix, the charges were mainly accumulated at the interfaces between MWCNTs particles and PDMS matrix, which established numerous microcapacitors and contributed to the enhancement of dielectric constant [54]. When the MWCNTs content reached up to 5 wt%, the real permittivity spectra exhibited obviously frequency dispersion behavior; namely, the dielectric constant decreased with the increase of frequency. Interestingly, the negative permittivity with a relatively small value was observed starting with 933 MHz (shown in Fig. 5(b)). In our previous investigations [55,56], the negative permittivity was achieved in metal/ceramic composites due to the plasma oscillation of the delocalized electrons in metallic clusters, which can be explained by Drude model [12]. Moreover, the plasma-like negative permittivity was obtained in polyimide/carbon nanotube composites [57], which was ascribed to the metallic-like nature of MWCNTs. In this PDMS/MWCNTs composite film, the real permittivity switched from positive to negative values with a dielectric resonance, which can be described by the Lorentz model as shown by equations (4) and (5) [58,59]:

$$\varepsilon = 1 + \frac{\omega_p^2}{\omega_0^2 - \omega^2 + i\omega\omega_\tau} \tag{4}$$

$$\omega_p = \sqrt{\frac{n_e e^2}{m_e \varepsilon_0}} \tag{5}$$

where ε is the complex permittivity, ω_τ is collision frequency (the inverse relaxation time $1/\tau$), ω is the angular frequency of external electric field, ω_0 is the characteristic frequency, ω_p is plasma frequency, n_e is the effective concentration of conductive electrons, m_e is the effective mass of electron and ε_0 is the permittivity of vacuum.

When the frequency of external electric field f and the intrinsic frequency of materials f_0 possess the same or similar frequency, the dielectric resonance took place and the negative permittivity appeared [59]. It is worth noting that the resonance characteristic was not very distinct, which was attributed to the huge damping coefficient. In addition, similar negative permittivity behavior was observed in the MWCNTs/polypropylene composites [19] and Ag/Al_2O_3 composites [60]. It was also suggested that the interband transition can be responsible for the positive-negative permittivity transition [19]. In our future research, more attention should be paid to the membranous composites with more functional filler content and tunable negative permittivity behavior.

For heterogeneous composites with conductive fillers, the dissipation factor ε"$_r$ depends on the conductive carriers and polarizing dipoles especially in the vicinity of percolation threshold [61]. Hence, the dielectric loss ε"$_r$ from the combined contributions of conduction and polarization can be expressed as equation **(6)** [44],

$$\varepsilon_r'' = \varepsilon_c'' + \varepsilon_p'' = \frac{\sigma}{\omega\varepsilon_0} + \frac{\varepsilon_s - \varepsilon_\infty}{1 + \omega^2\tau^2} \tag{6}$$

where ω is angular frequency, σ is dc conductivity, τ is relaxation time, ε_0, ε_s and ε_∞ is the vacuum, static and high-frequency dielectric constant, respectively. ε_c"and ε_p"represent the dissipation in the form of conductivity and polarization, respectively.

In the composites with low MWCNTs loadings, the imaginary permittivity presented weak dielectric loss in the test frequency

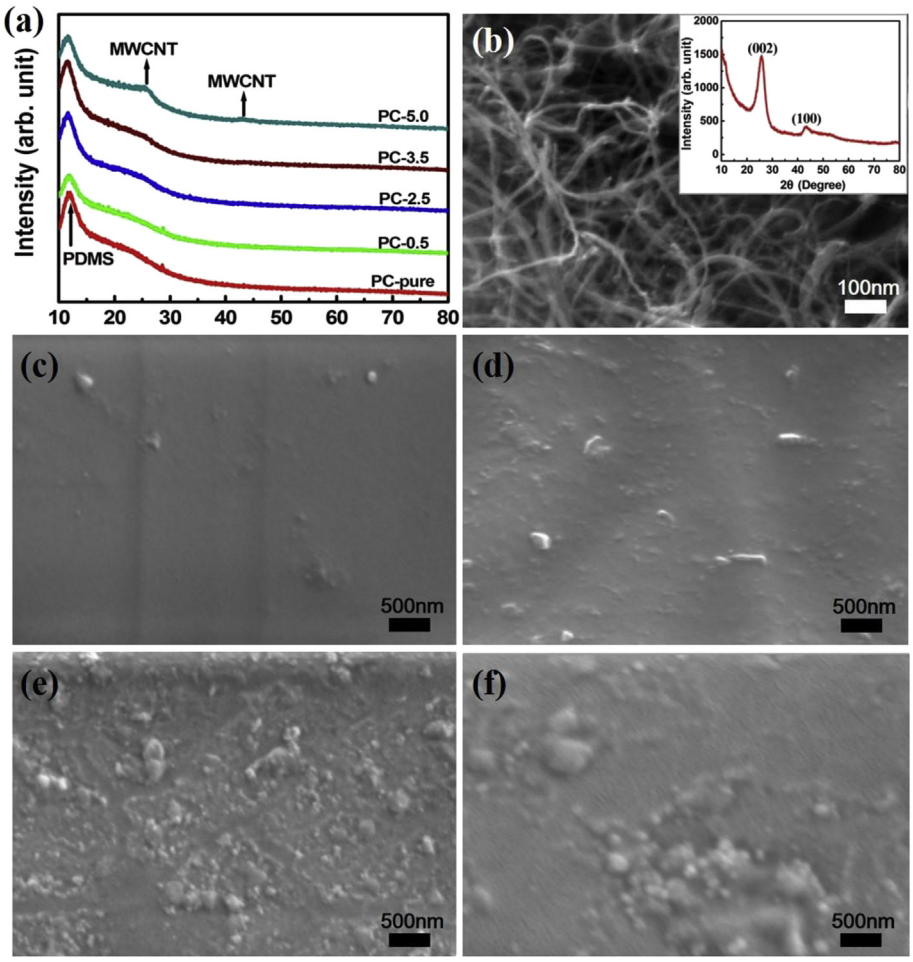

Fig. 3. The XRD patterns (a) and the microstructures of PDMS/MWCNTs composites with different mass fractions of carbon nanotubes: (b) 0, (c) 0.5, (d) 2.5, (e) 3.5 and (f) 5.0 wt%. The inset in (b) shows the XRD pattern of pure MWCNTs.

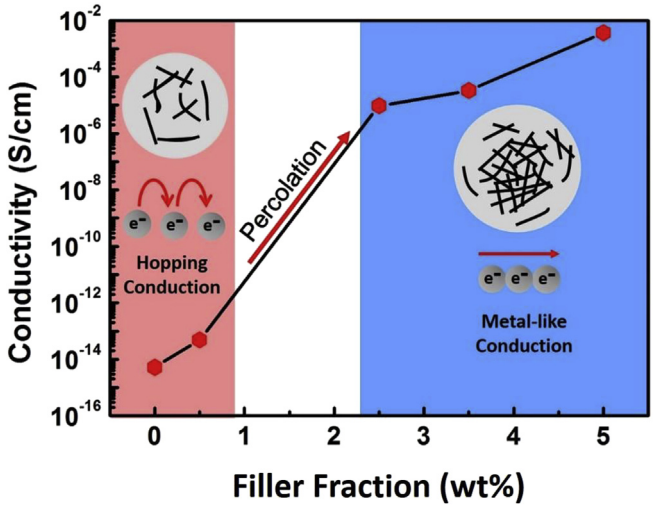

Fig. 4. The dependence of dc conductivity on filler fraction in PDMS/MWCNTs films. The insets present the different distributions of MWCNTs in PDMS films, and the two forms of electrons conduction, respectively.

region, indicating that the frequency response from the insulating matrix became dominant for the composites with a low carbon nanotubes loading level [62]. When the conductive MWCNTs fraction was above 2.5 wt%, there exists some leakage current produced resulting from the agglomerated one-dimension MWCNTs fillers. In this case, the PDMS/MWCNTs composites present metal-like behavior and possess lower breakdown strength, which have potential applications in microwave absorbing, electromagnetic attenuation and shielding fields. As shown in Fig. 5(c), the dielectric loss ε" and frequency f conformed to linear relation, *i.e.*, $\varepsilon_r'' \propto 1/f$, indicating that the conductive carriers played a primary role in dielectric loss for the composites with high carbon nanotubes contents [63]. For the composites with 5 wt% MWCNTs fillers, the imaginary permittivity spectrum showed an apparent difference from others. As shown in Fig. 5(d), there was a linear relation between ε"$_r$ and frequency f, which demonstrated that conduction played an overwhelming role in the dielectric dissipation. With the increase of frequency, the energy loss was gradually dominated by polarizing dipoles rather than the conduction electrons, so the permittivity exhibited the relaxation characteristic [44]. Similar phenomena were also observed in the Ni/epoxy composites [61] and MWCNTs/Al_2O_3 composites [59].

Fig. 5(e)-5(f) shows the dielectric loss tangent ($\tan\delta = \varepsilon$"$_r/\varepsilon'_r$) of the PDMS/MWCNTs composites. When the MWCNTs content was below 5 wt%, although there existed a leakage current derived from the partial CNTs networks, the $\tan\delta$ was not too large to hamper the impedance match, compared with that of previous study [63,64]. For the resultant composites with negative permittivity (shown in Fig. 5(f)), the dielectric loss peak was achieved at the resonance

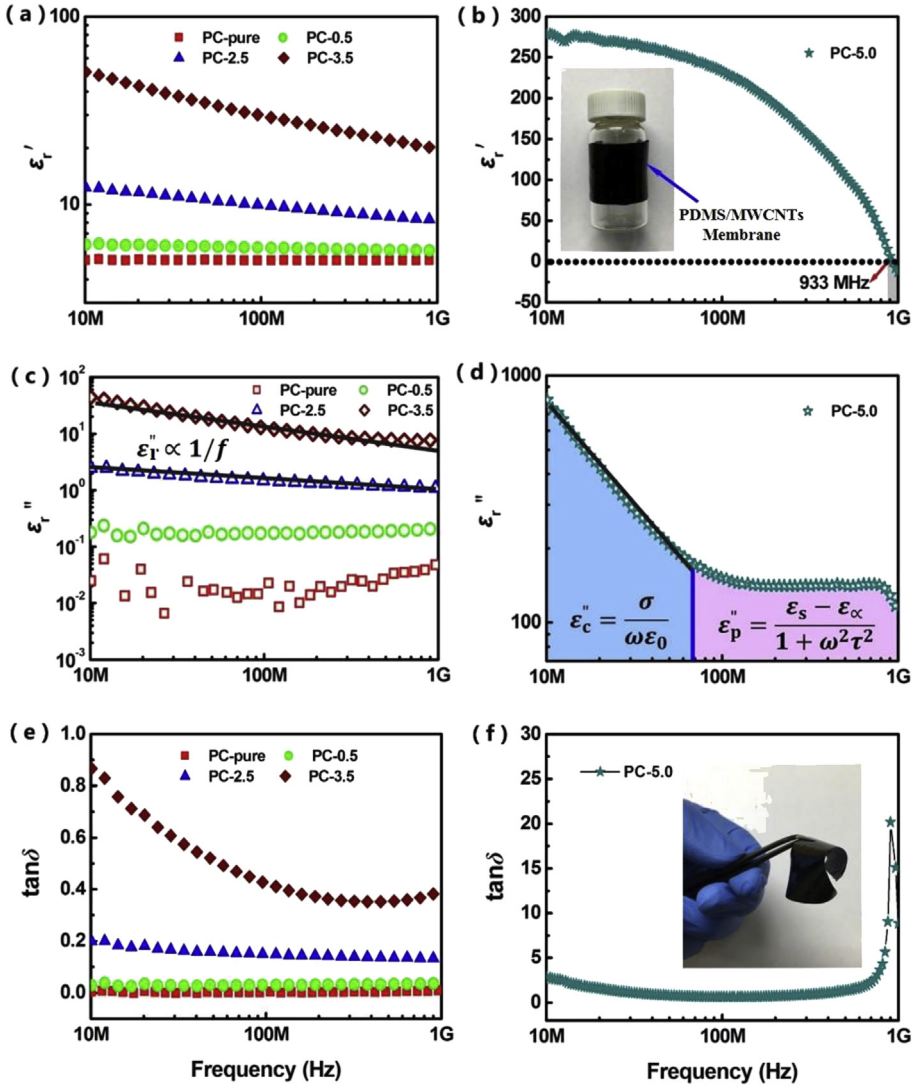

Fig. 5. The dielectric dispersion of the complex permittivity for PDMS/MWCNTs composite films. (a) and (b) the real permittivity spectra; (c) and (d) the imaginary permittivity spactra; (e) and (f) the dielectric loss tangent. The inset in (b) shows that the PDMS/MWCNTs membranous metacomposite with 5 wt% MWCNTs fillers is wrapped around the glass bottle. The inset in (f) shows the flexibility of PDMS/MWCNTs membranous metacomposite.

frequency, where the real permittivity changed from positive to negative values. Additionally, seen from the insets in Fig. 5(b) and (f), the PDMS/MWCNTs membranous metacomposites were wrapped around the surface of glass bottle and presented excellent flexibility, which can be promising candidate for wearable cloaks [21] and flexible devices [24]. It is significant to improve the dielectric property taking advantage of functional MWCNTs [65]. Moreover, it could be an alternative to search for flexible membrane with other functional fillers [66–68].

4. Conclusions

Flexible PDMS/MWCNTs membranous nanocomposites were fabricated via in-situ polymerization process; the conductivity and the complex permittivity were further investigated. When the conductive MWCNTs fillers reached percolated state, there was an electrical percolation phenomenon attained owing to the formed conductive networks. It was demonstrated that the conductive mechanism changed from hopping conduction to metal-like conduction in the vicinity of percolation threshold. Furthermore, the dielectric dispersion behavior of the PDMS/MWCNTs composites was investigated based on the spectra of complex permittivity. It was revealed that the dielectric loss was dominated by conduction and polarization in the heterogeneous composites with conductive fillers. The negative permittivity was obtained at the resonance frequency, which was attributed to the induced electric dipoles. It was indicated that the interband transition was responsible for the positive-negative permittivity transition. Hopefully, the flexible PDMS/MWCNTs metacomposite films have significant applications, especially in the field of wearable cloaks, sensing, perfect absorption and stretchable electronic devices.

Acknowledgements

The authors acknowledge the supports of National Natural Science Foundation of China (Grant No. 51402271, No.51601105), Natural Science Foundation of Shandong Province (No. ZR2016EMM09) and China Scholarship Council.

References

[1] D.R. Smith, J.B. Pendry, M.C. Wiltshire, Metamaterials and negative refractive

index, Science 305 (2004) 788–792.
[2] J. Valentine, S. Zhang, T. Zentgraf, E. Ulin-Avila, D.A. Genov, G. Bartal, X. Zhang, Three-dimensional optical metamaterial with a negative refractive index, Nature 455 (2008) 376–379.
[3] V.G. Veselago, The electrodynamics of substances with simultaneously negative values of ε and μ, Sov. Phys. Usp. 10 (1968) 509.
[4] D. Schurig, J. Mock, B. Justice, S.A. Cummer, J.B. Pendry, A. Starr, D. Smith, Metamaterial electromagnetic cloak at microwave frequencies, Science 314 (2006) 977–980.
[5] J.B. Pendry, Negative refraction makes a perfect lens, Phys. Rev. Lett. 85 (2000) 3966.
[6] B. Wang, K.H. Teo, T. Nishino, W. Yerazunis, J. Barnwell, J. Zhang, Experiments on wireless power transfer with metamaterials, Appl. Phys. Lett. 98 (2011) 254101.
[7] M.J. Freire, R. Marques, L. Jelinek, Experimental demonstration of a μ=−1 metamaterial lens for magnetic resonance imaging, Appl. Phys. Lett. 93 (2008) 231108.
[8] H. Chen, Metamaterials: constitutive parameters, performance, and chemical methods for realization, J. Mater. Chem. 21 (2011) 6452–6463.
[9] M. Chen, X. Wang, Z. Zhang, K. Sun, C. Cheng, F. Dang, Negative permittivity behavior and magnetic properties of C/YIG composites at radio frequency, Mater. Des. 97 (2016) 454–458.
[10] J. Zhu, S. Wei, L. Zhang, Y. Mao, J. Ryu, A.B. Karki, D.P. Young, Z. Guo, Polyaniline-tungsten oxide metacomposites with tunable electronic properties, J. Mater. Chem. 21 (2011) 342–348.
[11] T. Tsutaoka, T. Kasagi, S. Yamamoto, K. Hatakeyama, Low frequency plasmonic state and negative permittivity spectra of coagulated Cu granular composite materials in the percolation threshold, Appl. Phys. Lett. 102 (2013) 181904.
[12] Z. Shi, R. Fan, Z. Zhang, L. Qian, M. Gao, M. Zhang, L. Zheng, X. Zhang, L. Yin, Random composites of nickel networks supported by porous alumina toward double negative materials, Adv. Mater 24 (2012) 2349–2352.
[13] B. Li, G. Sui, W.H. Zhong, Single negative metamaterials in unstructured polymer nanocomposites toward selectable and controllable negative permittivity, Adv. Mater 21 (2009) 4176–4180.
[14] Z. Shi, R. Fan, Z. Zhang, K. Yan, X. Zhang, K. Sun, X. Liu, C. Wang, Experimental realization of simultaneous negative permittivity and permeability in Ag/$Y_3Fe_5O_{12}$ random composites, J. Mater. Chem. C 1 (2013) 1633–1637.
[15] P. Xie, K. Sun, Z. Wang, Y. Liu, R. Fan, Z. Zhang, G. Schumacher, Negative permittivity adjusted by SiO_2-coated metallic particles in percolative composites, J. Alloys Compd. (2017) (in press), https://doi-org.proxy.lib.utk.edu:2050/10.1016/j.jallcom.2017.04.248.
[16] J. Zhu, Z. Luo, S. Wu, N. Haldolaarachchige, D.P. Young, S. Wei, Z. Guo, Magnetic graphene nanocomposites: electron conduction, giant magnetoresistance and tunable negative permittivity, J. Mater. Chem. 22 (2012) 835–844.
[17] C. Cheng, K. Yan, R. Fan, L. Qian, Z. Zhang, K. Sun, M. Chen, Negative permittivity behavior in the carbon/silicon nitride composites prepared by impregnation-carbonization approach, Carbon 96 (2016) 678–684.
[18] J. Zhu, S. Wei, N. Haldolaarachchige, J. He, D.P. Young, Z. Guo, Very large magnetoresistive graphene disk with negative permittivity, Nanoscale 4 (2012) 152–156.
[19] X. Zhang, X. Yan, Q. He, H. Wei, J. Long, J. Guo, H. Gu, J. Yu, J. Liu, D. Ding, Electrically conductive polypropylene nanocomposites with negative permittivity at low carbon nanotube loading levels, ACS Appl. Mater. Inter 7 (2015) 6125–6138.
[20] H.D. Shetty, V. Prasad, Existence of negative permittivity in carbon coated iron nanoparticle-PDMS composites, Mater. Chem. Phys. 196 (2017) 153–159.
[21] S. Yang, P. Liu, M. Yang, Q. Wang, J. Song, L. Dong, From flexible and stretchable meta-atom to metamaterial: a wearable microwave meta-skin with tunable frequency selective and cloaking effects, Sci. Rep. 6 (2016).
[22] R. Melik, E. Unal, N. Kosku Perkgoz, C. Puttlitz, H.V. Demir, Flexible metamaterials for wireless strain sensing, Appl. Phys. Lett. 95 (2009) 181105.
[23] Y. Yoo, H. Zheng, Y. Kim, J. Rhee, J.-H. Kang, K. Kim, H. Cheong, Y. Kim, Y. Lee, Flexible and elastic metamaterial absorber for low frequency, based on small-size unit cell, Appl. Phys. Lett. 105 (2014) 041902.
[24] S. Hong, H. Lee, J. Lee, J. Kwon, S. Han, Y.D. Suh, H. Cho, J. Shin, J. Yeo, S.H. Ko, Highly stretchable and transparent metal nanowire heater for wearable electronics applications, Adv. Mater 27 (2015) 4744–4751.
[25] L. Hu, D.S. Hecht, G. Gruner, Carbon nanotube thin films: fabrication, properties, and applications, Chem. Rev. 110 (2010) 5790–5844.
[26] X. Yan, J. Gu, G. Zheng, J. Guo, A.M. Galaska, J. Yu, M.A. Khan, L. Sun, D.P. Young, Q. Zhang, Lowly loaded carbon nanotubes induced high electrical conductivity and giant magnetoresistance in ethylene/1-octene copolymers, Polymer 103 (2016) 315–327.
[27] I.W. Moran, A.L. Briseno, S. Loser, K.R. Carter, Device fabrication by easy soft imprint nano-lithography, Chem. Mater 20 (2008) 4595–4601.
[28] Z.M. Dang, T. Zhou, S.H. Yao, J.K. Yuan, J.W. Zha, H.T. Song, J.Y. Li, Q. Chen, W.T. Yang, J. Bai, Advanced calcium copper titanate/polyimide functional hybrid films with high dielectric permittivity, Adv. Mater 21 (2009) 2077–2082.
[29] K. Nomura, H. Ohta, A. Takagi, T. Kamiya, M. Hirano, H. Hosono, Room-temperature fabrication of transparent flexible thin-film transistors using amorphous oxide semiconductors, Nature 432 (2004) 488–492.
[30] S. Walia, C.M. Shah, P. Gutruf, H. Nili, D.R. Chowdhury, W. Withayachumnankul, M. Bhaskaran, S. Sriram, Flexible metasurfaces and metamaterials: a review of materials and fabrication processes at micro-and nano-scales, Appl. Phys. Rev. 2 (2015) 011303.
[31] K.C. Cheung, P. Renaud, H. Tanila, K. Djupsund, Flexible polyimide microelectrode array for in vivo recordings and current source density analysis, Biosens. Bioelectron. 22 (2007) 1783–1790.
[32] Y. Zheng, Y. Zheng, S. Yang, Z. Guo, T. Zhang, H. Song, Q. Shao, Esterification synthesis of ethyl oleate catalyzed by Brønsted acid–surfactant-combined ionic liquid, Green Chem. Lett. Rev. 10 (2017) 202–209.
[33] (a) Z. Sun, L. Zhang, F. Dang, Y. Liu, Z. Fei, Q. Shao, H. Lin, J. Guo, L. Xiang, N. Yerra, Experimental and simulation-based understanding of morphology controlled barium titanate nanoparticles under co-adsorption of surfactants, CrystEngComm 19 (2017) 3288–3298;
(b) K. Zhang, G. Li, L. Feng, N. Wang, J. Guo, K. Sun, K. Yu, J. Zeng, T. Li, Z. Guo, M. Wang, Ultralow percolation threshold and enhanced electromagnetic interference shielding in poly(L-lactide)/multi-walled carbon nanotubes nanocomposites with electrically conductive segregated networks, J. Mater. Chem. C. (2017), http://dx.doi.org/10.1039/C7TC02948A in press.
[34] C. Wang, Y. Wu, Y. Li, Q. Shao, X. Yan, C. Han, Z. Wang, Z. Liu, Z. Guo, Flame-retardant rigid polyurethane foam with a phosphorus-nitrogen single intumescent flame retardant, Polym. Adv. Technol. (2017). http://dx.doi.org/10.1002/pat.4105.
[35] T. Yamada, Y. Hayamizu, Y. Yamamoto, Y. Yomogida, A. Izadi-Najafabadi, D.N. Futaba, K. Hata, A stretchable carbon nanotube strain sensor for human-motion detection, Nat. Nanotechnol. 6 (2011) 296–301.
[36] J.M. Harris, G.R.S. Iyer, A.K. Bernhardt, J.Y. Huh, S.D. Hudson, J.A. Fagan, E.K. Hobbie, Electronic durability of flexible transparent films from type-specific single-wall carbon nanotubes, ACS Nano 6 (2011) 881–887.
[37] B. Tian, T. Cohen-Karni, Q. Qing, X. Duan, P. Xie, C.M. Lieber, Three-dimensional, flexible nanoscale field-effect transistors as localized bioprobes, Science 329 (2010) 830–834.
[38] J.N. Chazalviel, U.P. Rodrigues-Filho, On the νSiO infrared absorption of polysiloxane films, Thin Solid Films 520 (2012) 3918–3921.
[39] L. Wang, Q. Ji, T. Glass, T. Ward, J. McGrath, M. Muggli, G. Burns, U. Sorathia, Synthesis and characterization of organo siloxane modified segmented polyether polyurethanes, Polymer 41 (2000) 5083–5093.
[40] H. Hu, L. Zhao, J. Liu, Y. Liu, J. Cheng, J. Luo, Y. Liang, Y. Tao, X. Wang, J. Zhao, Enhanced dispersion of carbon nanotube in silicone rubber assisted by graphene, Polymer 53 (2012) 3378–3385.
[41] L. Liu, Z. Jiang, F. Pan, F. Peng, H. Wu, The unusual change of permeation rate in PDMS membranes filled with crystalline calixarene and its derivative, J. Membr. Sci. 279 (2006) 111–119.
[42] K. Sun, Z. Zhang, R. Fan, M. Chen, C. Cheng, Q. Hou, X. Zhang, Y. Liu, Random copper/yttrium iron garnet composites with tunable negative electromagnetic parameters prepared by in situ synthesis, RSC Adv. 5 (2015) 61155–61160.
[43] Z.M. Dang, J.K. Yuan, J.W. Zha, T. Zhou, S.T. Li, G.H. Hu, Fundamentals, processes and applications of high-permittivity polymer–matrix composites, Prog. Mater Sci. 57 (2012) 660–723.
[44] K. Sun, R. Fan, Y. Yin, J. Guo, X.-F. Li, Y. Lei, L. An, C. Cheng, Z. Guo, Tunable negative permittivity with fano-like resonance and magnetic property in percolative silver/yttrium iron garnet nanocomposites, J. Phys. Chem. C (2017) 7564–7571.
[45] C.W. Nan, Y. Shen, J. Ma, Physical properties of composites near percolation, Annu. Rev. Mater. Res. 40 (2010) 131–151.
[46] M. Surve, V. Pryamitsyn, V. Ganesan, Dispersion and percolation transitions of nanorods in polymer solutions, Macromolecules 40 (2007) 344–354.
[47] A. Ameli, M. Nofar, C. Park, P. Pötschke, G. Rizvi, Polypropylene/carbon nanotube nano/microcellular structures with high dielectric permittivity, low dielectric loss, and low percolation threshold, Carbon 71 (2014) 206–217.
[48] T. Prasse, J.-Y. Cavaille, W. Bauhofer, Electric anisotropy of carbon nanofibre/epoxy resin composites due to electric field induced alignment, Compos. Sci. Technol. 63 (2003) 1835–1841.
[49] K. Sau, T. Chaki, D. Khastgir, Conductive rubber composites from different blends of ethylene-propylene-diene rubber and nitrile rubber, J. Mater. Sci. 32 (1997) 5717–5724.
[50] S. Goffri, C. Müller, N. Stingelin-Stutzmann, D.W. Breiby, C.P. Radano, J.W. Andreasen, R. Thompson, R.A. Janssen, M.M. Nielsen, P. Smith, Multi-component semiconducting polymer systems with low crystallization-induced percolation threshold, Nat. Mater 5 (2006) 950–956.
[51] X. Wang, Z. Shi, M. Chen, R. Fan, K. Yan, K. Sun, S. Pan, M. Yu, Tunable electromagnetic properties in Co/Al_2O_3 cermets prepared by wet chemical method, J. Am. Ceram. Soc. 97 (2014) 3223–3229.
[52] Z. Shi, R. Fan, K. Yan, K. Sun, M. Zhang, C. Wang, X. Liu, X. Zhang, Preparation of iron networks hosted in porous alumina with tunable negative permittivity and permeability, Adv. Funct. Mater 23 (2013) 4123–4132.
[53] H. Gu, Y. Huang, X. Zhang, Q. Wang, J. Zhu, L. Shao, N. Haldolaarachchige, D.P. Young, S. Wei, Z. Guo, Magnetoresistive polyaniline-magnetite nanocomposites with negative dielectrical properties, Polymer 53 (2012) 801–809.
[54] N. Yousefi, X. Sun, X. Lin, X. Shen, J. Jia, B. Zhang, B. Tang, M. Chan, J.K. Kim, Highly aligned graphene/polymer nanocomposites with excellent dielectric properties for high-performance electromagnetic interference shielding, Adv. Mater 26 (2014) 5480–5487.
[55] K. Sun, R. Fan, Z. Zhang, K. Yan, X. Zhang, P. Xie, M. Yu, S. Pan, The tunable negative permittivity and negative permeability of percolative Fe/Al_2O_3 composites in radio frequency range, Appl. Phys. Lett. 106 (2015) 172902.
[56] K. Sun, Z. Zhang, L. Qian, F. Dang, X. Zhang, R. Fan, Dual percolation behaviors of electrical and thermal conductivity in metal-ceramic composites, Appl.

Phys. Lett. 108 (2016) 061903.
[57] Y. Sun, J. Wang, S. Qi, G. Tian, D. Wu, Permittivity transition from highly positive to negative: polyimide/carbon nanotube composite's dielectric behavior around percolation threshold, Appl. Phys. Lett. 107 (2015) 012905.
[58] K. Yan, R. Fan, M. Chen, K. Sun, L. Yin, H. Li, S. Pan, M. Yu, Perovskite (La, Sr) MnO_3 with tunable electrical properties by the Sr-doping effect, J. Alloys Compd. 628 (2015) 429–432.
[59] C. Cheng, R. Fan, Y. Ren, T. Ding, L. Qian, J. Guo, X. Li, L. An, Y. Lei, Y. Yin, Radio frequency negative permittivity in random carbon nanotubes/alumina nanocomposites, Nanoscale 9 (2017) 5779–5787.
[60] Z. Shi, F. Mao, J. Wang, R. Fan, X. Wang, Percolative silver/alumina composites with radio frequency dielectric resonance-induced negative permittivity, RSC Adv. 5 (2015) 107307–107312.
[61] Z. Wang, W. Zhou, L. Dong, X. Sui, H. Cai, J. Zuo, Q. Chen, Dielectric spectroscopy characterization of relaxation process in Ni/epoxy composites, J. Alloys Compd. 682 (2016) 738–745.
[62] G. Tsangaris, N. Kouloumbi, S. Kyvelidis, Interfacial relaxation phenomena in particulate composites of epoxy resin with copper or iron particles, Mater. Chem. Phys. 44 (1996) 245–250.
[63] C. Wu, X. Huang, X. Wu, L. Xie, K. Yang, P. Jiang, Graphene oxide-encapsulated carbon nanotube hybrids for high dielectric performance nanocomposites with enhanced energy storage density, Nanoscale 5 (2013) 3847–3855.
[64] X. Yao, X. Kou, J. Qiu, M. Moloney, Generation mechanism of negative dielectric properties of metallic oxide crystals/polyaniline composites, J. Phys. Chem. C 120 (2016) 4937–4944.
[65] L. Shao, Y. Bai, X. Huang, Z. Gao, L. Meng, Y. Huang, J. Ma, Multi-walled carbon nanotubes (MWCNTs) functionalized with amino groups by reacting with supercritical ammonia fluids, Mater. Chem. Phys. 116 (2009) 323–326.
[66] (a) X. Yang, X. Jiang, Y. Huang, Z. Guo, L. Shao, Building nanoporous metal–organic frameworks "Armor" on fibers for high-performance composite materials, ACS Appl. Mater. Inter. 9 (2017) 5590–5599;
(b) T. Wu, Q. Shao, S. Ge, The facile preparation of novel magnetic zirconia composites with the aid of carboxymethyl chitosan and their efficient removal of dye, RSC Adv. 6 (2016) 58020–58027;
(c) W. Zhu, S. Ge, Q. Shao, Adsorption properties of ZrO_2 hollow microboxes prepared using $CaCO_3$ cubes as templates, RSC Adv. 6 (2016) 81736–81743;
(d) S. Ge, X. Yang, Q. Shao, Q. Liu, T. Wang, L. Wang, X. Wang, Self-assembled flower-like antimony trioxide microstructures with high infrared reflectance performance, J. Solid State Chem. 200 (2013) 136–142.
[67] X. Jiang, S. Li, L. Shao, Pushing CO_2-philic membrane performance to the limit by designing semi-interpenetrating networks (SIPN) for sustainable CO_2 separations, Energy Environ. Sci. 10 (2017) 1339–1344.
[68] Y. Li, X. Wu, J. Song, J. Li, Q. Shao, N. Cao, N. Lu, Z. Guo, Reparation of recycled acrylonitrile-butadiene-styrene by pyromellitic dianhydride: reparation performance evaluation and property analysis, Polymer 124 (2017) 41–47.